




# c-Maf enforces cytokine production and promotes memory-like responses in mouse and human type 2 innate lymphoid cells

Sara Trabanelli<sup>1,‡,§</sup>, Giuseppe Ercolano<sup>1,\*</sup> , Tania Wyss<sup>1</sup>, Alejandra Gomez-Cadena<sup>1,‡,§</sup>, Maryline Falquet<sup>1,‡,§</sup>, Daniela Cropp<sup>1</sup>, Claire Imbratta<sup>2,#</sup>, Marine M Leblond<sup>1</sup>, Valentina Salvestrini<sup>3</sup>, Antonio Curti<sup>3</sup>, Olivier Adotevi<sup>4</sup>, Camilla Jandus<sup>1,\*</sup> , & Grégory Verdeil<sup>1,\*\*</sup> 

## Abstract

Group-2 innate lymphoid cells (ILC2s), which are involved in type 2 inflammatory diseases such as allergy, can exhibit immunological memory, but the basis of this ILC2 “trained immunity” has remained unclear. Here, we found that stimulation with IL-33/IL-25 or exposure to the allergen papain induces the expression of the transcription factor c-Maf in mouse ILC2s. Chronic papain exposure results in high production of IL-5 and IL-13 cytokines and lung eosinophil recruitment, effects that are blocked by c-Maf deletion in ILCs. Transcriptomic analysis revealed that knockdown of c-Maf in ILC2s suppresses expression of type 2 cytokine genes, as well as of genes linked to a memory-like phenotype. Consistently, c-Maf was found highly expressed in human adult ILC2s but absent in cord blood and was required for cytokine production in isolated human ILC2s. Furthermore, c-Maf-deficient mouse or human ILC2s failed to exhibit strengthened (“trained”) responses upon repeated challenge. Thus, the expression of c-Maf is indispensable for optimal type 2 cytokine production and proper memory-like responses in ILC2s.

**Keywords** c-Maf; ILC2; immune training; lung inflammation

**Subject Category** Immunology

**DOI** 10.15252/emboj.2021109300 | Received 27 July 2021 | Revised 31 March 2022 | Accepted 1 April 2022

**The EMBO Journal (2022) e109300**

## Introduction

Innate lymphoid cells (ILCs) play major roles in early physiological and pathological processes by producing a large amount of a broad spectrum of cytokines and soluble mediators (Vivier *et al*, 2018). Mirroring the nomenclature of T helper (Th) CD4<sup>+</sup> T cells, ILCs have been termed ILC1s, ILC2s, and ILC3s (ILCPs if referring to human peripheral blood; Lim *et al*, 2017), with high plasticity among the different subsets (Colonna, 2018; Vivier *et al*, 2018). ILC2s coordinate type 2 inflammatory responses by the prompt secretion of Th2 cytokines such as IL-13 and IL-5. While *GATA3*, *Nfil3*, *Bcl11b*, and *Rora* have emerged as master regulators of ILC2 commitment and differentiation (Hoyler *et al*, 2012; Yu *et al*, 2015; Ferreira *et al*, 2021), much less is known on the transcriptional programs controlling mature ILC2 functions. Moreover, while traditionally, immunological memory has been considered a prerequisite of adaptive immune cells, it has recently become evident that natural killer cells, as well as ILC2s, do form memory responses (Martinez-Gonzalez *et al*, 2016; Dominguez-Andres & Netea, 2020). Yet, the molecular mechanisms underlying ILC2 “trained immunity” remain poorly understood.

Recently, it has been shown that the transcription factor c-Maf, expressed early during murine ILC differentiation (Harly *et al*, 2018), is also present in mature intestinal ILC3s, particularly in CCR6<sup>+</sup>NKp46<sup>+</sup> cells (Pokrovskii *et al*, 2019; Parker *et al*, 2020; Tizian *et al*, 2020), where it regulates the ILC3/ILC1 balance. In that context, c-Maf promotes ILC3 identity by upregulating canonical type 3 inflammation-associated genes and by directly inhibiting T-bet expression, thus repressing ILC1 conversion (Parker *et al*,

<sup>1</sup> Department of Oncology, UNIL-CHUV, Ludwig Institute for Cancer Research Lausanne, University of Lausanne, Lausanne, Switzerland

<sup>2</sup> Department of Oncology, UNIL-CHUV, University of Lausanne, Lausanne, Switzerland

<sup>3</sup> IRCCS Azienda Ospedaliero-Universitaria di Bologna, Istituto di Ematologia “Seràgnoli”, Bologna, Italy

<sup>4</sup> INSERM, UMR1098 RIGHT, EFS-BFC, University of Bourgogne Franche-Comté, Besançon, France

\*Corresponding author. Tel: +41 22 379 5440; E-mail: camilla.jandus@unige.ch

\*\*Corresponding author. Tel: +41 21 692 5989; E-mail: gregory.verdeil@unil.ch

<sup>†</sup>These authors contributed equally to this work

<sup>‡</sup>Present address: Department of Pathology and Immunology, Faculty of Medicine, University of Geneva, Geneva, Switzerland

<sup>§</sup>Present address: Ludwig Institute for Cancer Research, Lausanne Branch, Lausanne, Switzerland

<sup>#</sup>Present address: Department of Pharmacy, University of Naples Federico II, Naples, Italy

<sup>¶</sup>Present address: Department of Pathology, South African Tuberculosis Vaccine Initiative, Institute of Infectious Disease and Molecular Medicine, Division of Immunology, University of Cape Town, Cape Town, South Africa

2020). Conversely, transcriptomic profiling of human ILCs identified c-Maf as most highly expressed in ILC2s, suggesting a function for c-Maf also in this ILC lineage (Bjorklund *et al*, 2016). In line with that, it has been recently reported that, in mouse ILC2s, c-Maf regulates IL-10 production in ILC2s (Howard *et al*, 2020) and can be targeted by miR-155 (Zhu *et al*, 2020).

Here, by combining mouse and human studies and by analyzing the transcriptional profile of c-Maf-competent and c-Maf-deficient ILC2s, we identified c-Maf as a key transcription factor enforcing the type 2 functional identity of ILC2s and determining their ability to develop trained features. c-Maf-deficient ILC2s are impaired in type 2 cytokine secretion, are unable to mount a stronger response upon antigen re-challenge, and lose the expression of several type 2 inflammation-related genes. Thus, our data define c-Maf as a key regulator of ILC2 identity, by enforcing their type 2 commitment.

## Results

### Human ILC2s (hILC2s) express c-Maf

Within the ILCs, c-Maf was shown to be expressed at early stage during ILC differentiation (Harly *et al*, 2018) and in mature intestinal murine ILC3s (Parker *et al*, 2020). However, in humans, c-Maf transcripts were preferentially found in ILC2s (hILC2s; Bjorklund *et al*, 2016). To explore the role of c-Maf in hILC2s, we evaluated its protein expression within circulating ILCs. In peripheral blood, hILC2s expressed higher levels of c-Maf compared with hILC1s or hILCPs (Fig 1A and B and Appendix Fig S1), suggesting that c-Maf could play a role in this lineage. Moreover, c-Maf expression varied within the hILC2 compartment, being higher in the cKit<sup>low</sup> than in the cKit<sup>high</sup> hILC2s (Bernink *et al*, 2019; Hochdorfer *et al*, 2019; Fig 1C and D). These data indicate that c-Maf is upregulated in fully mature and lineage committed hILC2s, but it is also highly expressed in the hILC2s that can have hILC3 features (Bernink *et al*, 2019; Hochdorfer *et al*, 2019). This pattern suggests that c-Maf may regulate hILC2 functions.

### Mouse ILC2s (mILC2s) lack c-Maf at steady-state, but express it upon stimulation

To study the role of c-Maf in ILC2s *in vivo*, we monitored c-Maf expression in murine ILC subsets. c-Maf expression was analyzed in different organs of wild-type C57BL/6 mice including blood, lymph node (LN), spleen, lungs, and gut. In contrast to hILC2s, at steady-state, c-Maf was not expressed by mILC2s in any of the organ analyzed, but rather in mILC3s, as previously described (Parker *et al*, 2020; Fig 2A and B). However, because our human data suggested preferential expression of c-Maf in fully mature ILC2s, we stimulated mILC2 using cytokines and/or known ILC2 triggers. Mice were treated with IL-33, IL-25, TSLP, or PGD2 and then sacrificed to analyze c-Maf expression as well as mILC2 subset distribution according to their expression of ST2 and KLRG1. As expected, upon IL-33 and IL-25 stimulation natural mILC2s (ST2<sup>+</sup>KLRG1<sup>-</sup>) were decreased in favor of KLRG1<sup>+</sup> mILC2 (Fig 2C and D). IL-33 preferentially induced ST2<sup>+</sup>KLRG1<sup>+</sup> activated ILC2s, while IL-25 preferentially induced inflammatory ILC2s (ST2<sup>-</sup>KLRG1<sup>+</sup>; Huang

*et al*, 2015; Zhang *et al*, 2017). In both cases, c-Maf was upregulated in mILC2s (Fig 2E and F), indicating that, upon ILC2 activation, c-Maf is expressed independently from the ILC2 subset analyzed (Appendix Fig S2A). No effect was observed upon TSLP and PGD2 stimulation (Fig 2C–F), and on the other mILC subsets (Appendix Fig S2A and B), suggesting that c-Maf expression is low in steady-state mILC2s, and only induced by a defined set of specific signals.

### c-Maf regulates ILC2 cytokine production

To study the role of c-Maf in mILC2s and hILC2s, we bred mice harboring a floxed *Maf* gene (*Maf*<sup>fl/fl</sup>) with mice expressing or not a tamoxifen inducible Cre recombinase under the Id2 promoter (Id2-Cre<sup>ERT2</sup>), which is known to control ILC development and is expressed in all ILCs (Ishizuka *et al*, 2016). Mice treated with tamoxifen received IL-33 to induce c-Maf in the ILC2s present in different organs (Fig 3A and Appendix Fig S3). This resulted in c-Maf induction in Id2-Cre<sup>ERT2</sup>-*Maf*<sup>fl/fl</sup> mice (c-Maf wild-type (WT)) and in c-Maf induction and simultaneous deletion in Id2-Cre<sup>ERT2</sup>+*Maf*<sup>fl/fl</sup> mice (c-Maf KO). In similar conditions, we showed by using Id2-Cre<sup>ERT2</sup>+ crossed on a Rosa-TdTomato reporter strain that the only cell type for which the Id2 promoter is highly active on top of ILCs is NK cells. As NK cells do not express c-Maf, off-target effects are unlikely to occur in our settings (Appendix Fig S4A and B). Differently from GATA3, c-Maf knockdown did not affect ILC2s' frequency, number, nor their activation status (Fig 3B and Appendix Fig S5A–C). In parallel, we infected peripheral blood hILC2s with a lentiviral vector-based shRNA construct against c-Maf (*Maf*-sh) or luciferase (*Luc*-sh) as control, containing GFP to track and isolate the transduced hILC2s (Fig 3C). Transduction resulted in c-Maf decrease in the *Maf*-sh hILC2s at both RNA and protein level (Fig 3D and E).

ST2<sup>+</sup>KLRG1<sup>+</sup> mILC2s were isolated from the lung of c-Maf WT or c-Maf KO mice, and GFP<sup>+</sup> hILC2s were purified from transduced ILC2s. Cells were stimulated *in vitro* with IL-33, to compare their ability to produce type 2 cytokines and IL-10 (Howard *et al*, 2021). As shown in Fig 3F and G, c-Maf sustains type 2 cytokine and IL-10 production in both mouse and human ILC2s, as independently from the species, c-Maf decrease resulted in an impaired secretion of IL-13, IL-5, and IL-10 (and IL-9 only in mice).

### c-Maf drives ILC2 functions during allergic responses

Next, we investigated whether c-Maf was induced and able to drive ILC2 functions in a physiological model of lung inflammation, such as upon acute and chronic allergen challenge. We used intranasal papain administration for 5 consecutive days to induce acute inflammation, followed by one week of resting and another 5 consecutive days of papain administration to induce chronic inflammation (Fig 4A). The chronic papain stimulation resulted in higher c-Maf upregulation in mILC2s, ST2<sup>+</sup>KLRG1<sup>+</sup> ILC2 accumulation in the lungs, IL-13 and IL-5 production and eosinophil recruitment, in comparison with the acute stimulation (Fig 4B–E). We used the chronic inflammation model to investigate the effect of c-Maf deletion in a pathophysiologic setting (Fig 4F). As shown in Fig 4G, c-Maf was properly knocked down during the chronic

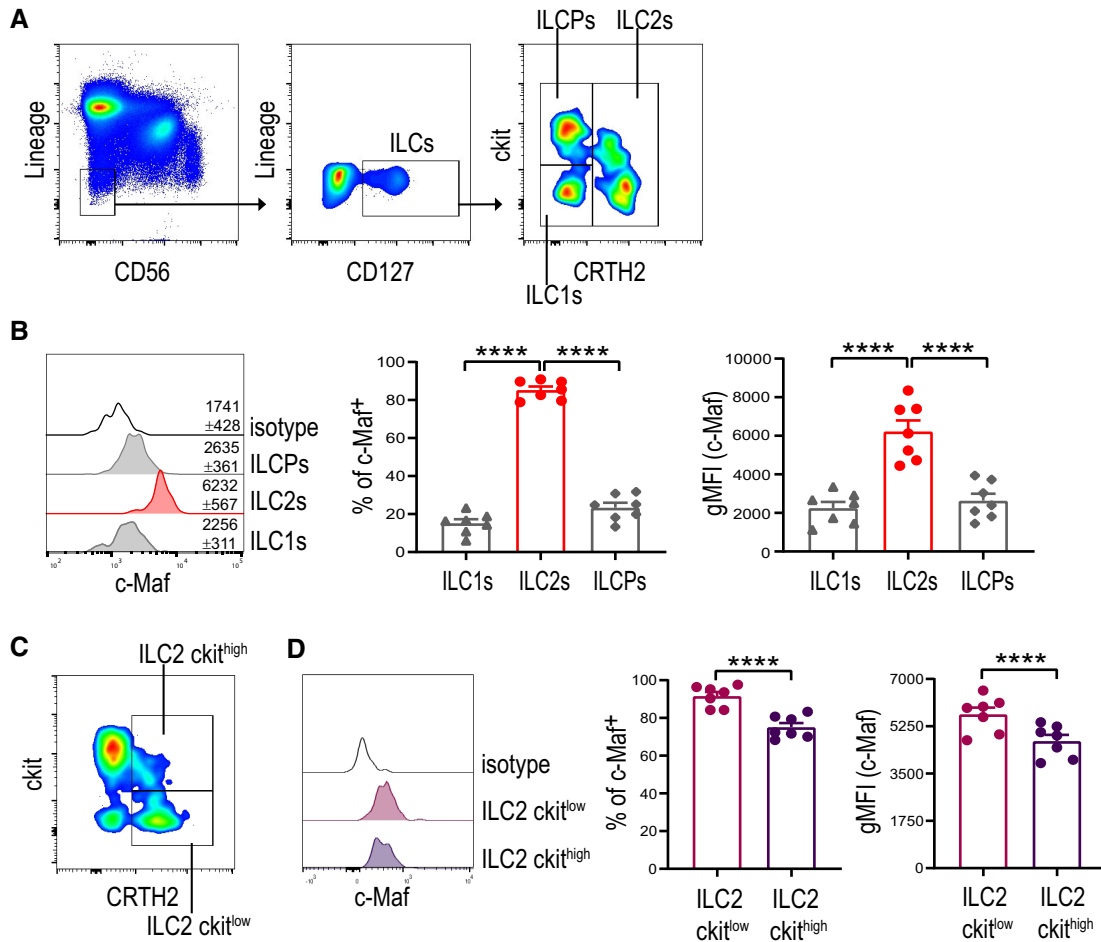


**Figure 1. Human ILC2s express high level of c-Maf.**

**A** Gating strategy used to identify ILCs and ILC subsets in humans (hILCs).

**B** Representative histogram and summary of the percentage and of the gMFI of c-Maf expression in hILC subsets (ANOVA analysis:  $F(2, 18) = 305.4$ , \*\*\*\* $P < 0.0001$ ).

**C, D** Gating strategy for cKit<sup>low</sup> and cKit<sup>high</sup> ILC2s (**C**) and expression level (percentage and gMFI) of c-Maf in cKit<sup>low</sup> and cKit<sup>high</sup> ILC2s (**D**) (paired *T* tests, \*\*\*\* $P < 0.0001$ ).

Data information: Each dot represents the expression level in one donor ( $n = 7$ ). Bars represent mean  $\pm$  SEM.

allergen challenge in the Id2-Cre<sup>ERT2+</sup>c-Maf<sup>fl/fl</sup> mice. c-Maf downregulation did not affect the accumulation of ST2<sup>+</sup>KLRG1<sup>+</sup> ILC2s in the lungs, while it resulted in their impaired capacity of secreting type 2 cytokines and of recruiting eosinophils (Fig 4H–J, Appendix Fig S5D). In line with these results, histological analysis of lung tissue revealed a higher inflammatory cell recruitment in the Id2-Cre<sup>ERT2-</sup> Maf<sup>fl/fl</sup> compared with the Id2-Cre<sup>ERT2+</sup> Maf<sup>fl/fl</sup> mice (Fig 4K).

### c-Maf regulates type 2 inflammation and innate memory genes

To uncover c-Maf-dependent genes regulating ILC2 functional identity, we performed differential gene expression analysis using bulk RNA-sequencing (RNA-seq) of ST2<sup>+</sup>KLRG1<sup>+</sup> ILC2s isolated from the lungs of Id2-Cre<sup>ERT2-</sup> Maf<sup>fl/fl</sup> and Id2-Cre<sup>ERT2+</sup> Maf<sup>fl/fl</sup> mice upon chronic papain stimulation and tamoxifen injections. Principal component analysis showed that c-Maf knocked-down ILC2s cluster

**Figure 2. c-Maf is inducible in mouse ILC2s.**

**A** Gating strategy used to identify ILCs and ILC subsets in mice (mILCs).

**B** Representative histogram and summary from 2 pooled independent experiments of the percentage of c-Maf expression in mILC subsets in the indicated organs (each symbol represents one individual biological replicate; ANOVA lung:  $F(2, 12) = 20.86$ ,  $P = 0.0001$ ; gut:  $F(2,12) = 22.27$ ,  $P < 0.0001$ ; spleen:  $F(2,12) = 4.705$ ,  $P = 0.031$ ; Kruskal–Wallis test LN:  $K = 9.815$ ,  $P = 0.0011$ ). Bars represent mean  $\pm$  SEM.

**C–F** Mice received the indicated compound for 3 consecutive days and lung ILCs were analyzed by flow cytometry the following day. Expression of ST2, KLRG1, and c-Maf was assessed in ILC2s. (**C**) Representative dot plots and histograms and (**D–F**) average from 2 pooled independent experiments for (**D**) the percentage of ST2<sup>+</sup>KLRG1<sup>+</sup>, ST2<sup>-</sup>KLRG1<sup>+</sup>, ST2<sup>-</sup>KLRG1<sup>-</sup>, ST2<sup>-</sup>KLRG1<sup>-</sup> ILC2s (2way ANOVA, interaction:  $F(12,56) = 13.82$ ,  $P < 0.0001$ ) and (**E**) the percentage and (**F**) the gMFI of c-Maf<sup>+</sup> ILC2s (Kruskal–Wallis test:  $K = 14.56$ ,  $P = 0.0057$ ). Each symbol represents one individual biological replicate. Bars represent mean  $\pm$  SEM.

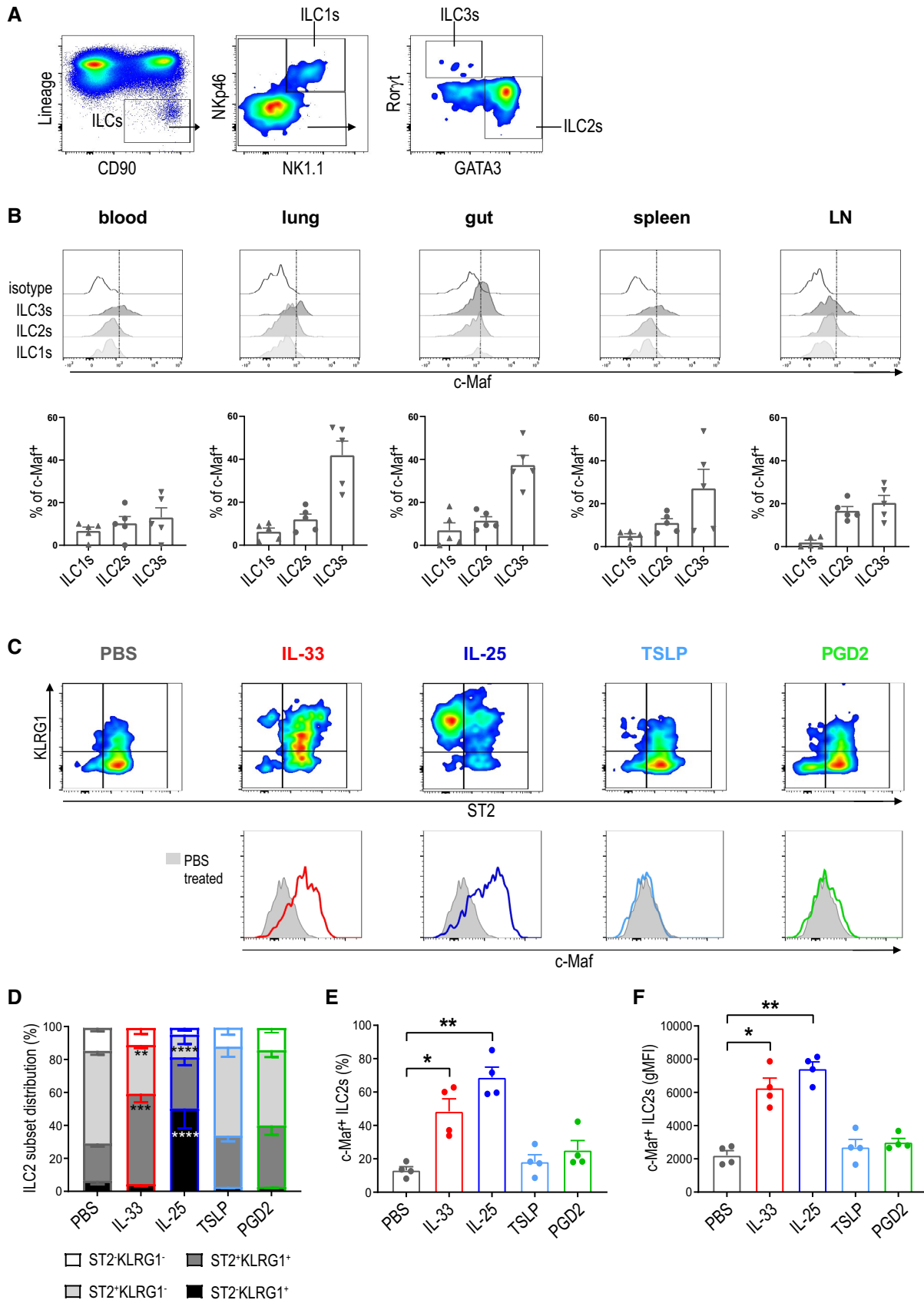
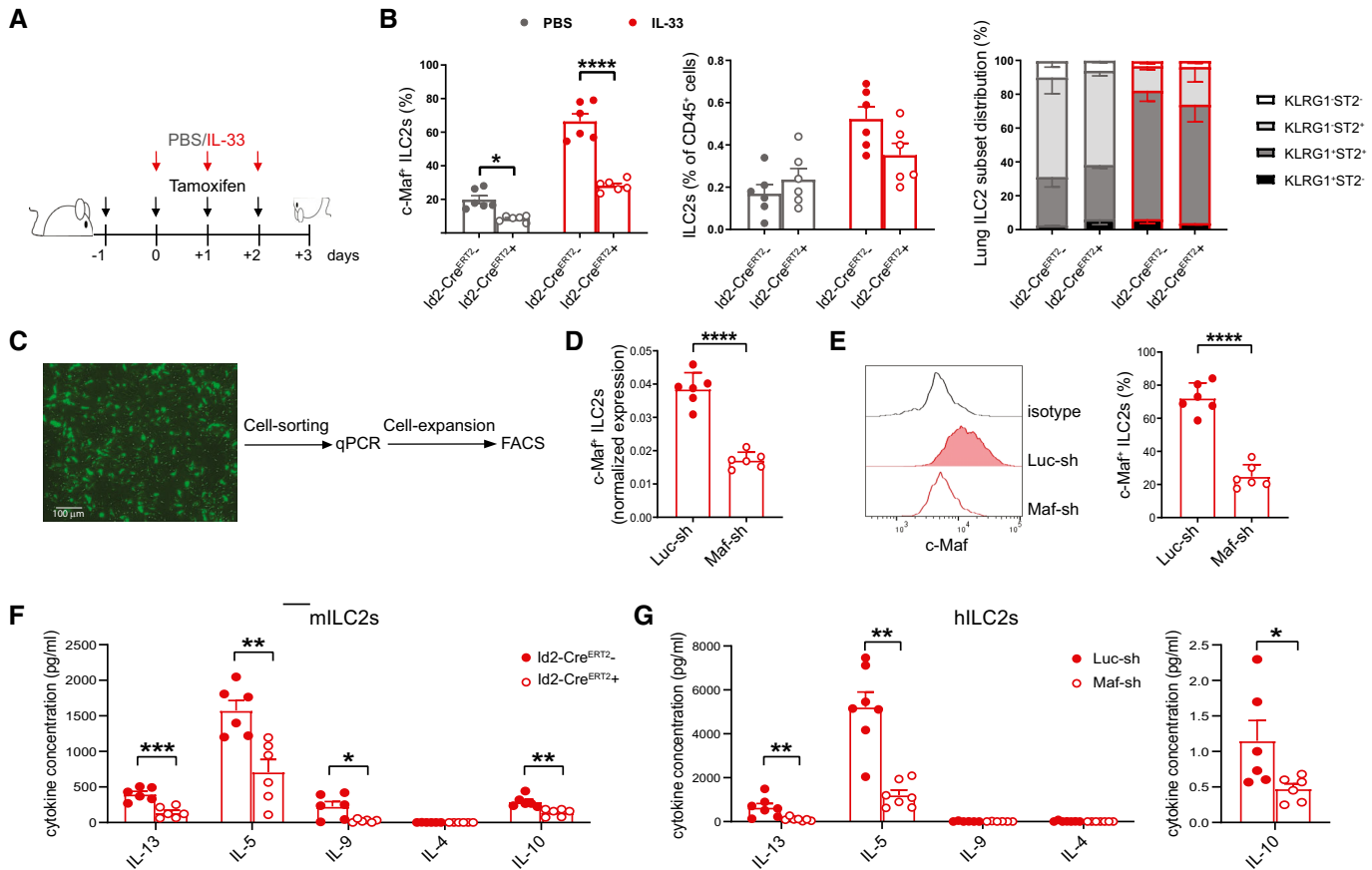


Figure 2.



**Figure 3. c-Maf deletion in mouse and human ILC2s dampens the production of ILC2-associated cytokines.**

- A Schedule for the injections of Tamoxifen and PBS or IL-33 in *Id2-Cre<sup>ERT2+</sup>* (*Id2-Cre<sup>+</sup>*) or *Id2-Cre<sup>ERT2-</sup>* (*Id2-Cre<sup>-</sup>*) *c-Maf<sup>fl/fl</sup>* mice.
- B Level of *c-Maf* (2way ANOVA, interaction:  $F(1,20) = 26.07$ , \*\*\*\* $P < 0.0001$ ), percentage of lung ILC2s among  $CD45^+$  cells and level of activation of lung ILC2s in *Id2-Cre<sup>+</sup> Maf<sup>fl/fl</sup>* (*c-Maf* WT) and *Id2-Cre<sup>-</sup> Maf<sup>fl/fl</sup>* (*c-Maf* KO) mice after treatment as indicated in (A). Bars represent mean  $\pm$  SEM.
- C Workflow after transduction of hILC2s with shRNA.
- D, E Relative mRNA level of *c-Maf* (T test, \*\*\*\* $P < 0.0001$ ) (D), representative histogram, and summary of the percentages of *c-Maf<sup>+</sup>* ILC2s transduced with a control (Luc-sh) or a *c-Maf* targeting shRNA (Maf-sh) (E). Isotype indicates staining with the isotype control of the anti-*c-Maf* Ab (T test, \*\*\*\* $P < 0.0001$ ). Bars represent mean  $\pm$  SEM.
- F Following the schedule indicated in (A), ILC2s were sorted from mouse lungs and stimulated for 48 h with IL-33. Concentration of the indicated cytokines in the supernatants was measured (Multiple Mann–Whitney tests). (T test, \* $P < 0.05$ , \*\* $P < 0.01$ , \*\*\* $P < 0.001$ ) Bars represent mean  $\pm$  SEM.
- G Human ILC2 sorted from peripheral blood and *in vitro* expanded were transduced with Luc-sh or Maf-sh as in (C). hILC2s were then stimulated for 48 h with IL-33, and the concentration of the indicated cytokines in the supernatants was measured (multiple Mann–Whitney tests, \* $P < 0.05$ , \*\* $P < 0.01$ ) Bars represent mean  $\pm$  SEM.

Data information: Each dot represents data from one individual mouse or from one donor.

separately from their wild-type counterparts along the first principal component, demonstrating that *c-Maf* shapes the transcriptome of ILC2s (Fig 5A). We identified 3,654 genes as being differentially expressed, with 2,335 upregulated and 1,319 downregulated genes, in the ILC2s of mice with a wild-type *c-Maf* (*Id2-Cre<sup>ERT2+</sup> Maf<sup>fl/fl</sup>*; absolute fold change  $> 3$ ; adjusted  $P$ -value  $< 0.02$ ; Fig 5B and Table EV1 for the gene list). Consistently with our flow cytometry data, ILC2s isolated from *c-Maf*-knock-down mice did not differ in the expression of ILC2 characterizing genes (e.g., *Ly6A* (Sca-1), *Klrg1*, *Thy1* (CD90), *Il1rl1* (ST2), and *Gata3*). However, they showed a lower expression of type 2 cytokines, in comparison with wild-type mice at transcriptional levels (*Il4*, *Il5*, and *Il13*, Fig 5B), highlighting a type 2 functional impairment. To better understand the amplitude of the type 2 impairment, we performed

an over-representation analysis using  $CD4^+$  T helper (Th) gene signatures (Stubington *et al*, 2015; Lee *et al*, 2016). Th2 genes were strongly upregulated in wild-type compared with *c-Maf* knocked-down ILC2s (Fig 5C and Table EV2 for the gene list), revealing that, in mILC2s, *c-Maf* expression strongly stabilized their type 2 signature. The downregulation of Th2-associated cytokines in *c-Maf* knocked-down ILC2s might be at least in part a direct consequence of the binding of *c-Maf* to the promoters of these cytokines. *In silico* search of the *c-Maf* DNA binding profile in the mouse genome identified potential motif matches within the IL-5, IL-13, and IL-4 promoters, and within open chromatin regions upstream of the promoters (Fig 5D). This indicates that *c-Maf* could directly interact with the IL-4, IL-5, and IL-13 promoters, as already demonstrated for IL-4 in Th2  $CD4^+$  cells (Kim *et al*, 1999). To substantiate this

finding, we performed chromatin immunoprecipitation (ChIP) on human and mouse expanded ILC2s stimulated or not with IL-33. The results indicated that c-Maf was directly bound to the promoter of IL-13, IL-5, and IL-4 in human and mouse ILC2s (Fig 5E).

To investigate the global c-Maf-dependent changes in gene expression programs, we performed an over-representation analysis against the Gene Ontology (GO) gene sets. Our analysis revealed a striking difference in genes involved in protein catabolic process that

were upregulated in the c-Maf-competent ILC2s (Fig 5F). In line with that, c-Maf wild-type ILC2s showed a better mitochondrial fitness than c-Maf knocked-down ILC2s (Appendix Fig S6A and B). Because metabolic changes are needed to induce immunological memory (Bekkering *et al*, 2018) and because a second exposure to papain resulted in a stronger induction of c-Maf leading to a higher production of cytokines (see Fig 4D), we hypothesized that c-Maf expression in ILC2s was linked to the formation of innate immunological

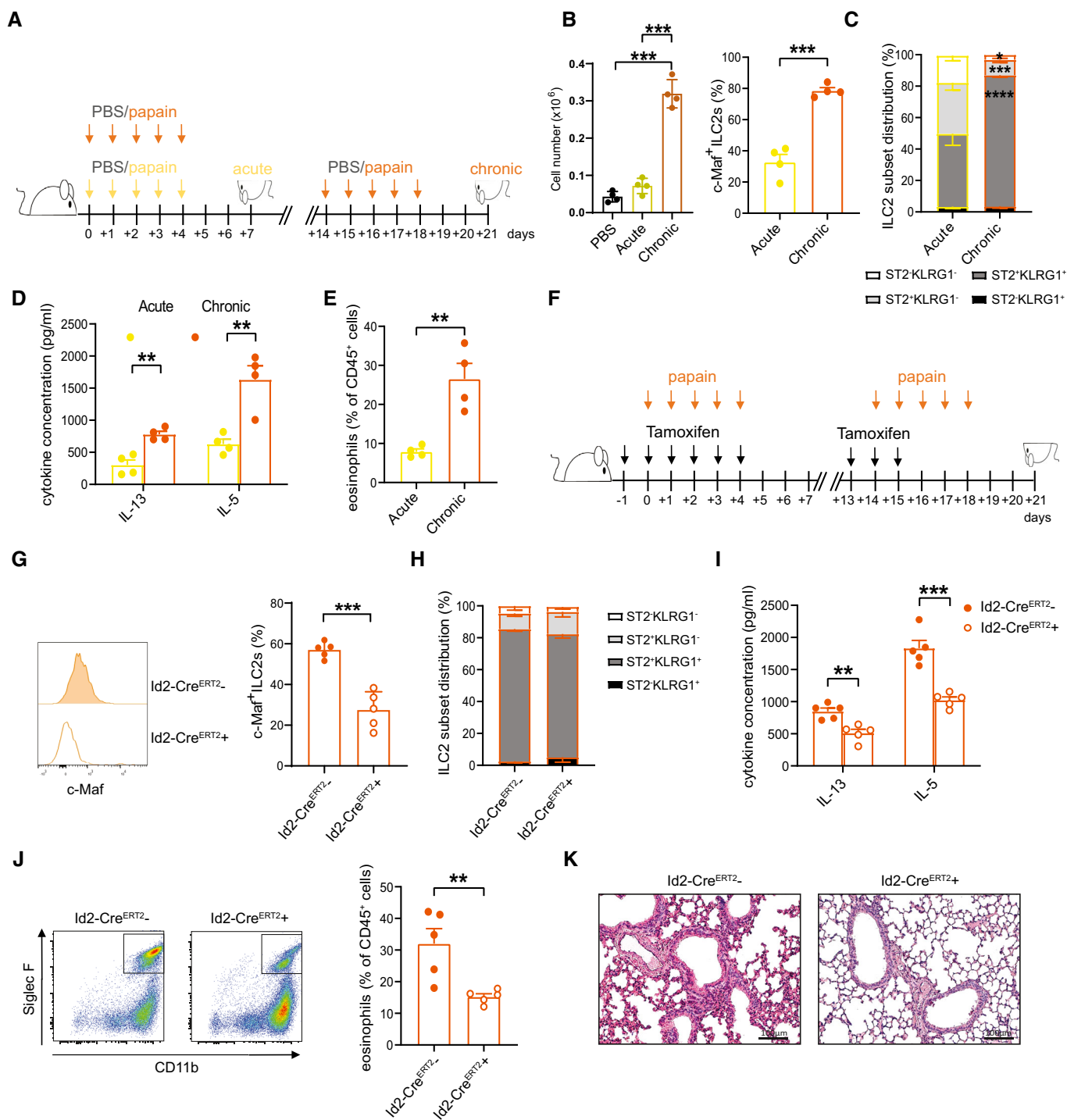


Figure 4.

**Figure 4. c-Maf knockdown in ILC2s dampens papain-induced lung inflammation.**

- A Treatment schedule for acute or chronic papain-induced lung inflammation.
- B, C Number of total ILC2s and percentage of c-Maf<sup>+</sup> (T test, \*\*\**P* < 0.001) (B); activation status of ILC2s (2way ANOVA, interaction: *F*(3,24) = 27.44, *P* < 0.0001) (C) from lungs after acute or chronic papain-induced lung inflammation (\**P* < 0.05, \*\*\**P* < 0.001, \*\*\*\**P* < 0.0001). Bars represent mean ± SEM.
- D IL-13 and IL-5 secretion of ILC2s sorted from lungs after acute or chronic papain-induced lung inflammation, stimulated for 48 h with IL-33 (multiple T tests, IL-13: \*\**P* = 0.0019; IL-5, \*\**P* = 0.0047). Bars represent mean ± SEM.
- E Percentage of eosinophils (Siglec-F<sup>+</sup>CD11b<sup>+</sup> cells) among CD45<sup>+</sup> cells was measured after acute or chronic papain-induced lung inflammation (T test, \*\**P* = 0.0038). Bars represent mean ± SEM.
- F Id2-Cre<sup>ERT2-</sup> Maf<sup>fl/fl</sup> and Id2-Cre<sup>ERT2+</sup> Maf<sup>fl/fl</sup> mice were treated with tamoxifen and papain following the chronic schedule.
- G Representative histogram and summary of the percentage of c-Maf<sup>+</sup> ILC2s from lungs of treated mice (T test, \*\*\**P* = 0.0001). Bars represent mean ± SEM.
- H Activation status of lung ILC2s from 5 mice per condition treated as in (F). Bars represent mean ± SEM.
- I IL-13 and IL-5 secretion of sorted lung ILC2s after chronic papain-induced lung inflammation and 48 h stimulation with IL-33 (Multiple T tests, IL-13: \*\**P* = 0.0026; IL-5: \*\*\**P* = 0.00027). Bars represent mean ± SEM.
- J Representative dot plot and percentage of eosinophils (Siglec-F<sup>+</sup>CD11b<sup>+</sup> cells) among CD45<sup>+</sup> cells was determined after chronic papain-induced inflammation in the indicated mouse strain (T test, \*\**P* = 0.0088). Bars represent mean ± SEM.
- K Lungs from these mice were fixed and used for hematoxylin-eosin staining. Representative pictures from 5 mice for each genotype are shown.
- Data information: (B–E) are representative of 2 independent experiments.

memory (Dominguez-Andres & Netea, 2020). The analysis of differentially expressed genes revealed that c-Maf knocked-down ILC2s downregulated several genes involved in CD8<sup>+</sup> T cell and Th2 cell memory, strongly suggesting a link between c-Maf and ILC2 trained immunity (Fig 5G and Table EV2 for the gene lists).

**c-Maf regulates ILC2 immunological training in mice and humans**

To verify the hypothesis that c-Maf regulates ILC2 immunological training, we treated Id2-Cre<sup>ERT2-</sup> Maf<sup>fl/fl</sup> and Id2-Cre<sup>ERT2+</sup> Maf<sup>fl/fl</sup> mice with IL-33 and tamoxifen (or PBS as control) and subsequently, after 4 days of resting, with intranasal papain for 5 days (Fig 6A). Our results showed that the downregulation of c-Maf during the “priming” phase caused milder responses to papain (Fig 6B and C), comparable to the one obtained for mice treated with papain only, without affecting ILC2 frequency or number (Appendix Fig S5E). This confirms that in the presence of c-Maf, ILC2s are fully immunologically trained.

As reported above, differently from mILC2s, hILC2s circulating in the blood of healthy adult individuals constitutively expressed c-Maf (see Fig 1). Therefore, we hypothesized that c-Maf is constitutively

expressed in adult hILC2s because they are constantly trained to react to signals coming from the external environment, for example, allergens/viruses contained in the air and in the food. We analyzed ILC2s in the human cord blood where ILCs have been less exposed to potential stimuli. In line with our hypothesis, *ex vivo* cord blood hILC2s showed dramatically lower levels of c-Maf while maintaining the same level of GATA3 as compared to adult hILC2s (Fig 6C). Cord blood hILC2s were also comparable to adult hILC2s in terms of expression of specific ILC2 and ILC activation markers (Fig 6D). To verify that “naturally” c-Maf-deficient hILC2s were less able to produce type 2 cytokines because not fully trained, and that the induction/upregulation of c-Maf was resulting in higher cytokine production, we stimulated cord blood and adult hILC2s and analyzed c-Maf expression and cytokine production. As shown in Fig 6E and F, upon short-term stimulation (3 h), cord blood hILC2s remained c-Maf-deficient and produced—if any—less IL-13 and IL-5 in comparison with adult, c-Maf-competent, hILC2s. However, when the 3 h stimulation followed an o.n. priming in the presence of IL-33, cord blood hILC2s upregulated c-Maf to levels comparable with adult hILC2s and were able to produce higher amounts of IL-13 and IL-5. The same trend was also observed in adult hILC2s, where the

**Figure 5. c-Maf regulates Th2-associated gene expression in ILC2s.**

- A Principal component analysis of c-Maf knocked-down (empty circles) and WT (filled circles) mILC2s, performed using all genes (*n* = 13,855) detected by mRNA sequencing. Numbers indicate mouse IDs.
- B Volcano plot showing genes more expressed in mILC2s purified from Id2-Cre<sup>ERT2-</sup> c-Maf<sup>fl/fl</sup> mice (dark red), genes more expressed in mILC2s purified from Id2-Cre<sup>ERT2+</sup> c-Maf<sup>fl/fl</sup> mice (dark blue), and genes not significantly differentially expressed (gray). The horizontal dashed line depicts the significance threshold at BH-adj. *P*-value = 0.02, while the vertical dashed lines depict an absolute log<sub>2</sub>(fold change) threshold = 1.
- C Over-representation analysis of genes defining Th2, Th1, and Th17 cells (see Table EV2 for a list of genes included in each signature) either for genes upregulated or downregulated in c-Maf WT ILC2s versus c-Maf knocked-down ILC2s.
- D Genomic location of the top matches (red rectangles) of the mouse c-Maf binding profile (shown at the top) and of the MARE sequence identified by (Ho *et al*, 1996). Motif search was performed within 2 types of regions (purple rectangles): (i) The promoters of IL-4, IL-5, and IL-13, and (ii) within open chromatin regions identified in 2 replicates of lung ILC2s or lung Th2 cells (dark blue tracks). The ATAC sequencing data (shown as bigwig coverage tracks) were retrieved from GEO (GSE77695). For each match of the c-Maf binding motif, numbers in parentheses indicate the log-likelihood ratio score and the raw *P*-value calculated by the FIMO tool. The transcripts of each gene are shown at the bottom of each panel. Mouse genome = mm9 and Integrative Genomics Viewer = v.2.8.0 (Robinson *et al*, 2011).
- E ChIP-qPCR analysis of c-Maf occupancy on IL-4, IL-5, and IL-13 promoters in untreated mouse and human ILC2s (IL-2 stimulation) and in mouse and human ILC2s treated with IL-33 (*n* = 3 biological replicates).
- F Dot plot showing over-represented Gene Ontology gene sets among genes upregulated in wild-type compared with c-Maf knocked-down ILC2s. The color scale depicts the adjusted *P*-value, while the size of the dots and x-axis depict the absolute number or the proportion of upregulated genes included in each gene set, respectively.
- G Sum of z-scores per sample of all genes upregulated in ST2<sup>+</sup> Th2 cells and memory CD8<sup>+</sup> T cells (see Appendix Table EV2 for a list of genes). The central band indicates the median, the box encompasses the interquartile range, and the whiskers reach the values that are within a distance of 1.5 times the interquartile range (either from the lower or upper quartile). The heatmap shows the z-scores of memory CD8<sup>+</sup> T cell genes significantly downregulated in c-Maf knocked-down ILC2s.

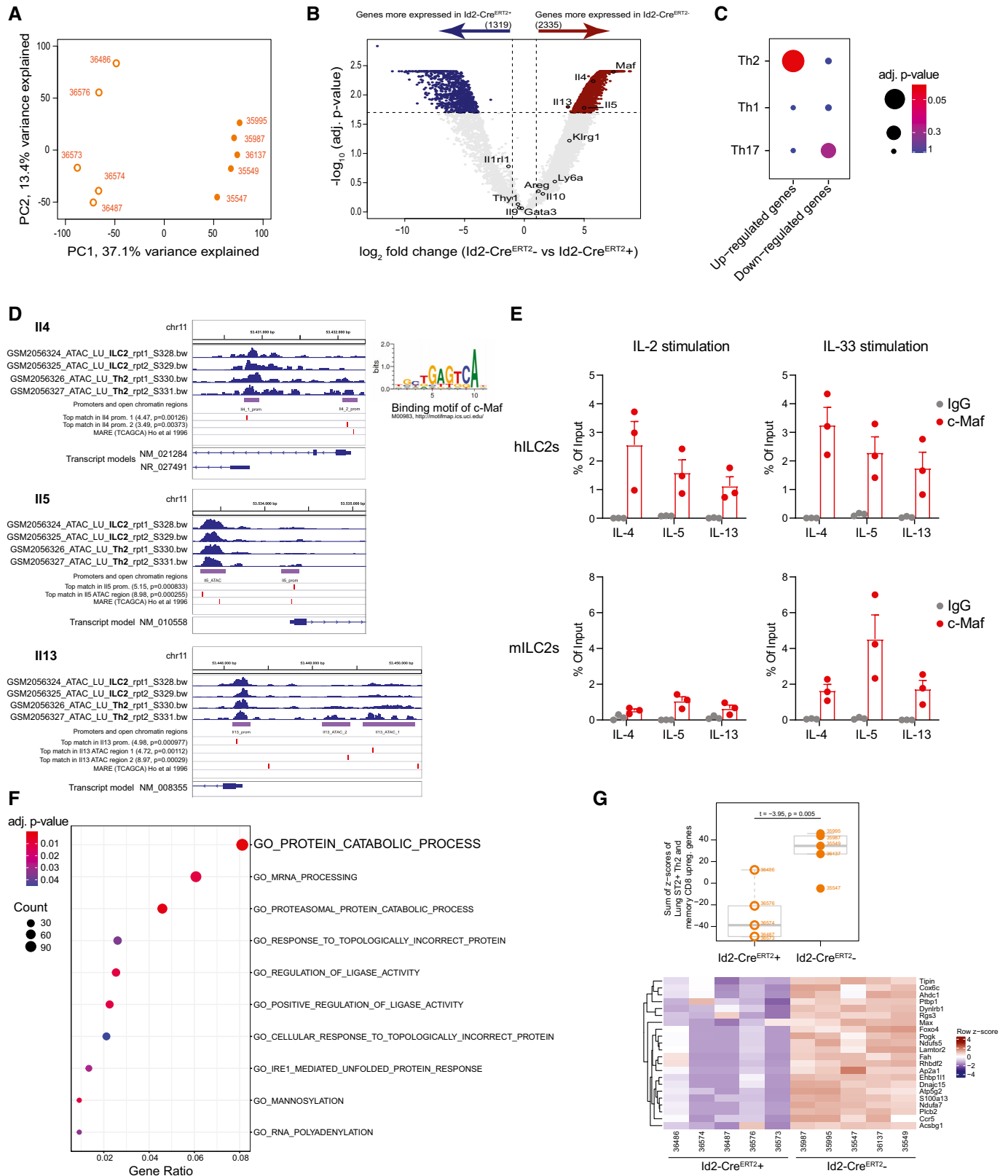
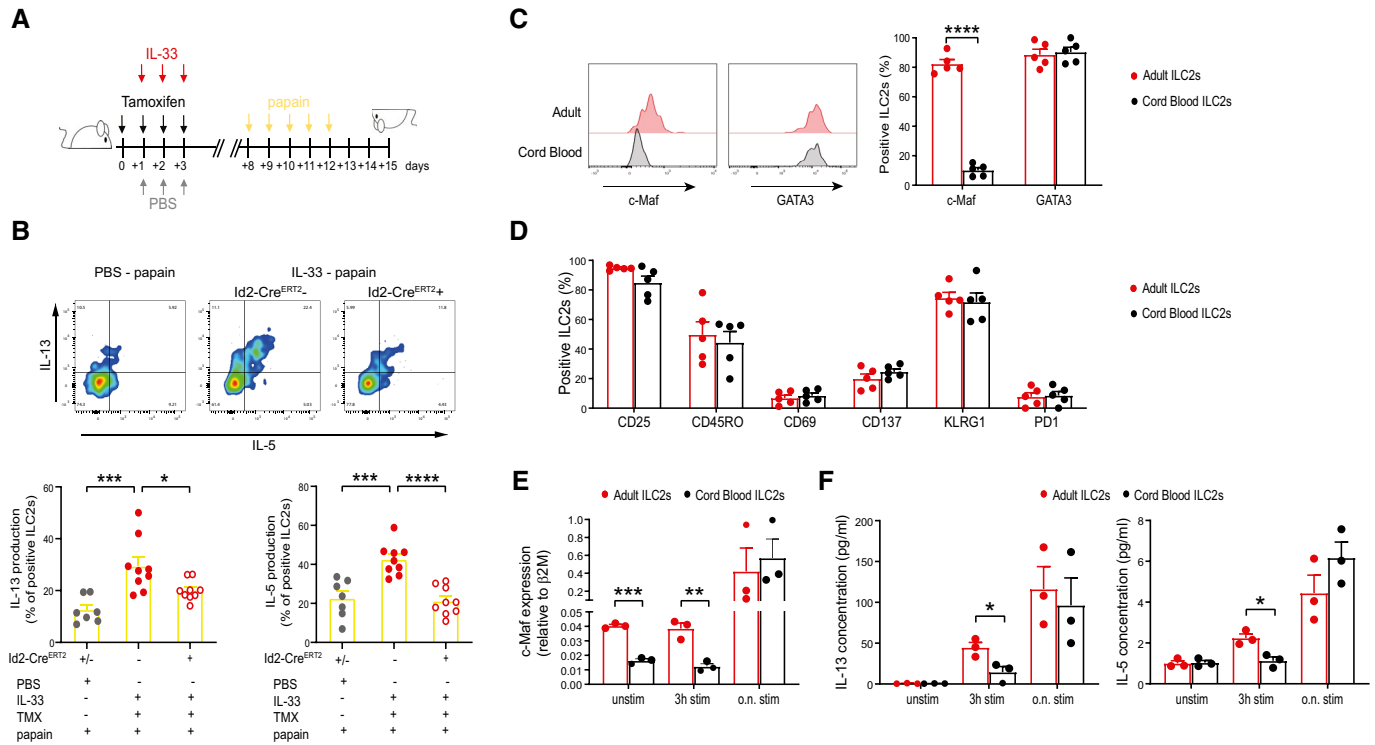


Figure 5.





**Figure 6. c-Maf induction enables ILC2s to respond stronger upon re-challenge.**

- A** Treatment schedule.
- B** Representative staining and percentage of IL-13<sup>+</sup> (ANOVA:  $F(2,22) = 11.37, P = 0.0004$ ) and IL-5<sup>+</sup> (ANOVA:  $F(2,22) = 18.05, P < 0.0001$ ) ILC2s after 3 h *in vitro* stimulation of cell suspension obtained from the lungs of mice treated as in (A). Each dot represents sample from one individual mouse (\* $P < 0.05$ , \*\*\*\* $P < 0.0001$ ). Bars represent mean  $\pm$  SEM.
- C** Representative histograms of c-Maf and GATA3 expression in ILC2s from adult PBMC or cord blood cells and percentages of c-Maf<sup>+</sup> and GATA3<sup>+</sup> ILC2s from adult PBMC or cord blood ( $n = 5$  different donors;  $T$  test, \*\*\*\* $P < 0.0001$ ).
- D** ILC2 expression of the indicated markers. Each dot represents sample from one donor. Bars represent mean  $\pm$  SEM.
- E** c-Maf quantification by qPCR (E) and cytokine concentration (F) in the supernatants of adult and cord blood ILC2s unstimulated, stimulated for 3 h with PMA-Ionomycin (3 h stim) and stimulated for an overnight with IL-33 and then 3 h with PMA-Ionomycin (o.n. stim). ILC2s were sorted from 3 different donors. (E) Multiple  $T$  tests, unstimulated:  $P = 0.000101$ ; 3 h stim:  $P = 0.0036$ . (F) Multiple  $T$  tests, IL-13:  $P = 0.022$ ; IL-5:  $P = 0.015$  (\* $P < 0.05$ ). Bars represent mean  $\pm$  SEM.

IL-33 priming resulted in a further upregulation of c-Maf and in a higher cytokine production.

These results demonstrate that, in the absence of environmental cues, ILC2s do not express c-Maf and are not fully functional. Upon c-Maf induction/upregulation, ILC2s gain a stronger capacity to produce type 2 cytokines.

## Discussion

In this study, by relating the expression of c-Maf to the functions of human and mouse ILC2s, we have uncovered a novel role for this transcription factor in stabilizing the type 2 functional differentiation of ILC2s. Our data are consistent with the identification of ILC2s expressing high level of c-Maf both in human and in mice (Bjorklund *et al*, 2016; Howard *et al*, 2020; Zhu *et al*, 2020) and extend those initial findings thanks to the transcriptomic and functional analysis of mouse and human c-Maf-competent and c-Maf-deficient ILC2s. We show that the absence of c-Maf in ILC2s results in a substantial loss of the type 2 transcriptional program, in impaired mitochondrial potential and in an incomplete capacity to

produce type 2 cytokines and IL-10. However, according to our transcriptional and flow cytometry analyses, c-Maf knocked-down ILC2s were not more prone to differentiate toward other ILC subsets. Indeed, differently from ILC3s, in which c-Maf was shown to regulate ILC3-ILC1 plasticity (Parker *et al*, 2020; Tizian *et al*, 2020), in ILC2s the absence of c-Maf did not induce the transcription of type 1 or type 3/17 genes (see Fig 5C and Table EV2). This likely excludes that, in ILC2s, the presence of c-Maf is a brake that impedes the switch of ILC2s toward a different subset, but rather enforces type 2 identity. Thus, c-Maf has a distinct role in ILC2s versus ILC3s.

Despite the presence of several differences at transcriptomic level, ILCs are considered the innate counterpart of CD4<sup>+</sup> T cells (Ercolano *et al*, 2020b). In CD4<sup>+</sup> T cells, c-Maf was first described as a major regulator of IL-4 expression in Th2 cells (Kim *et al*, 1999), before it was linked to other functions in different T cell subtypes (Giordano *et al*, 2015; Aschenbrenner *et al*, 2018; Gabrysova *et al*, 2018; Xu *et al*, 2018; Imbratta *et al*, 2019; Neumann *et al*, 2019). Our data showed that c-Maf knocked-down ILC2s were negatively affected in their capacity to produce IL-5 and IL-13 and, only at RNA level, IL-4, since c-Maf could bind directly their promoters (see Fig 5D and E).

Previous transcriptomic/epigenetic analysis of the role of c-Maf in CD4<sup>+</sup> T cells suggested that c-Maf is a transcription factor that stabilizes a transcriptional program already initiated by other master transcription factors (Gabrysova *et al*, 2018). In the case of ILC2s, our results suggest that, differently from GATA3, c-Maf is dispensable for ILC2 development, but enforces and stabilizes the expression of ILC2-associated genes and type 2-associated functions. Interestingly, the inactivation of c-Maf in ILC2s strongly attenuated papain-induced lung inflammation. This observation confirms the described role of ILC2s in the initiation of allergic reactions (Halim *et al*, 2012), highlighting the role of c-Maf in the regulation of cytokine production in the initial stages of allergic responses.

Interestingly, the protocol of chronic inflammation we used, with two rounds of papain administration, is reminiscent of a prime boost protocol used to induce ILC memory/training (Martinez-Gonzalez *et al*, 2016). By using an ILC2 memory/training signature similar to the one proposed by Martinez-Gonzalez *et al*, and combining it with the one characterizing memory Th2 cells (Rahimi *et al*, 2020), we unraveled that only c-Maf-competent ILC2s were able to upregulate core genes of trained immunity (see Fig 5G). This speculation was supported by the evidence that, when we first sensitized ILC2s with IL-33 and then re-challenged them with papain in the second step, we observed a strong increase in the capacity of ILC2s to produce IL-5 and IL-13 only in c-Maf-competent ILC2s, arguing for c-Maf expression as a marker of immunological training. In line with that, human non-trained ILC2s, that is, the ones circulating in an exclusively protected environment, such as the cord blood, showed very low levels of c-Maf expression and an impaired capacity of producing type 2 cytokines. On the contrary, human ILC2s isolated from adults showed a stable high level of c-Maf and a high cytokine production capacity, probably because of a continuous priming by environmental factors.

Therefore, our mouse and human data demonstrated that c-Maf is upregulated in ILC2s upon encounter with ILC2-triggering factor (s). Its expression results in the stabilization of the type 2 identity of ILC2s that gain the full competence to secrete type 2 cytokines during acute, chronic, and memory phases of the immune response.

## Materials and Methods

### Human samples

Venous blood was drawn from healthy donors at the local Blood Transfusion Center, Lausanne, Switzerland, under the approval of the Lausanne University Hospital's Institute Review Board. Fresh anticoagulated blood diluted at 1:2 ratio in PBS was layered on lymphoprep (ratio diluted blood:lymphoprep 1.5:1). Cord blood samples were collected at the French blood bank (Etablissement Français du Sang, BFC, Besançon, France) and at the University Hospital of Bologna (approval code: 94/2016/O/Tess) in anonymous fashion. Mononuclear cells were isolated by density gradient centrifugation (1,800 rpm, 20 min centrifugation without break, room temperature), washed, and immediately cryopreserved in 50% RPMI, 40% FCS, and 10% DMSO. Written informed consent was obtained from all the subjects, in accordance with the Declaration of Helsinki.

### Human ILC (hILC) isolation and FACS analysis

Isolated PBMCs were stained for 20 min at RT in sorting buffer (PBS, 50  $\mu$ M EDTA, 0.2% BSA) with the following specific, all FITC-conjugated lineage markers: anti-human CD3 (UCHT1, Beckman Coulter (BC)), anti-human CD4 (SFC12T4D11, BC), anti-human CD8 (MEM-31, Immunotools), anti-human CD14 (RMO52, BC), anti-human CD15 (80H5, BC), anti-human CD16 (3G8, Biolegend), anti-human CD19 (J3-119, BC), anti-human CD20 (2H7, Biolegend), anti-human CD33 (HIM3-4, Biolegend), anti-human CD34 (561, Biolegend), anti-human CD203c (E-NPP3) (NP4D6, Biolegend), anti-human Fc $\epsilon$ R1 $\alpha$  (AER-37, Biolegend). Additionally, we used: PC7 anti-human CD56 (5.1H11, Biolegend), Brilliant Violet 421 anti-human CD127 (A019D5, Biolegend), PerCP/Cy5.5 anti-human CRTH2 (BM16, Biolegend), APC anti-human cKit (104D2, Biolegend), and PE anti-mouse/human c-Maf (sym0F1, Invitrogen). To identify ILC3 and NK cells we also used: PC7 anti-human CXCR3 (1C6, BD Pharmingen), BV786 anti-human NKp44 (p44-8, BD Biosciences), BUV737 anti-human CD56 (NCAM16.2, BD Biosciences), and ECD anti-human CD16 (PN A33098, Beckman Coulter). Dead cells were excluded using the ViViD LIVE/DEAD fixable dead cell stain kit (LifeTechnologies). ILC2s were sorted as Lin<sup>+</sup>CD127<sup>+</sup>CRTH2<sup>+</sup> lymphocytes using a FACS Aria (Becton Dickinson). ILC2 phenotype was evaluated by using APC anti-GATA3 (16E10A23, Biolegend), BV605 anti-human cKit (104D2, Biolegend), AlexaFluor 647 anti-CRTH2 (BM16, Biolegend), PE anti-human KLRG1 (13F12F2, eBiosciences), PC7 anti-human CD25 (BC96, Biolegend), BUV737 anti-human CD69 (FN50, BD Biosciences), BV650 anti-human CCR6 (G034E3, Biolegend), BV711 anti-human PD1 (EH12.2H7, Biolegend), AlexaFluor 700 anti-human CD137 (4-1BB, Biolegend), and BV785 CD45RO (UCHL1, Biolegend). Samples were acquired on a Gallios flow cytometer (Beckman Coulter) or on a LSRFortessa (BD). Data were analyzed using FlowJo software (TreeStar V.10).

### Mouse ILC (mILC) isolation and FACS analysis

After collection, blood was incubated with red cell lysis buffer (Qiagen, 1 ml, 5 min, 37°C); cells were centrifuged and washed with PBS before the staining. Lungs were cut in small pieces and digested for 45 min in Collagenase D (Roche, 1 mg/ml). Single-cell suspensions were obtained by mashing organs through a 70  $\mu$ m cell strainer and were centrifuged in Percoll gradients 40%/70% for 20 min at 2,000 rpm. Gut was digested as described in Imbratta *et al* (2019). Briefly, gut was collected in HBSS (ThermoFisher Scientific) supplemented with 2% of fetal calf serum on ice. Samples were further flushed, cut, and treated with EDTA 1 mM (ThermoFisher Scientific) and DTT 1  $\mu$ M (AppliChem) in HBSS 10% solution for 20 min under shaking at 37°C. After intraepithelial lymphocyte removal, cells were incubated with Collagenase D (1 mg/ml) (Roche) and complete RPMI (ThermoFisher Scientific) at 37°C. To isolate leucocytes, supernatants were centrifuged in density gradients 40%/70% Percoll (GE Healthcare Life Sciences) for 30 min at 2,000 rpm. Spleen and lymph nodes were passed through a 70  $\mu$ m strainer. Single-cell suspensions were washed in PBS and stained with specific antibodies.

When indicated, mice were injected i.p. daily with 0.4  $\mu$ g of mouse IL-33 (Biolegend), mouse IL-25 (Roche), TSLP (peprotech), and PGD2 (Sigma) for 3 consecutive days. For papain treatment, mice received 20  $\mu$ g of papain (Carica papaya, Sigma-Aldrich) in

20  $\mu$ l of PBS intranasally as indicated in the schedules (see Fig 4A). Lungs were collected and digested, and the single-cell suspension was analyzed.

Isolated mononuclear cells were stained for 20 min at RT in sorting buffer (PBS, 50  $\mu$ M EDTA, 0.2% BSA) with the following specific, all FITC-conjugated lineage markers produced by the flow cytometry facility at UNIL unless indicated: anti-mouse CD3 (2C11), CD5 (53.7) CD8 (53.6.7) TCRab (H57-597, Biolegend) TCRgt (GL3) CD11b (M1/70), CD11c (HL3, eBioscience), B220 (RA3-6B2), CD19 (ID3), Ter119 (Ter119), DX5 (PanNK, Myltenyi); APC anti-mouse ST2 (RMST2-2, Invitrogen), APC-Cy7 anti-mouse CD127 (A7R34, Biolegend), BV605 anti-mouse CD90.2 (53-2.1, Biolegend), PE-Cy7 anti-mouse/human KLRG1 (2F1/KLRG1, Biolegend), PE anti-mouse/human c-Maf (sym0F1, Invitrogen), PerCP-eF710 anti-human/mouse GATA3 (TWAJ, Invitrogen), PE-eF610 anti-mouse ROR $\gamma$ t (B2D, Invitrogen) PE-Cy7 anti mouse NK1.1 (PK136, eBioscience), BV510 anti-mouse NKp46 (29A1.4, Biolegend), BV421 anti-mouse Siglec-F (E50-2440, BD), and BV650 CD11b (M1/70, Biolegend). For mitochondrial potential, lineage markers were used in APC from Myltenyi: anti-CD11b (M1/70.15.11.5), anti-CD11c (REA754), anti-CD3 (REA641), anti-CD5 (53-7.3), anti-CD8 (53 6.7), anti-CD19 (6D5), anti-B220 (RA3-6B2), anti-CD49b (DX5), anti-Ter119 (Ter119), anti-TCRg/d (GL3), anti-TCRb (REA318), and anti-FceRIa (MAR1). For cell sorting, mILC2s (lin<sup>-</sup>CD90.2<sup>+</sup>ST2<sup>+</sup>KLRG1<sup>-</sup>, lin<sup>-</sup>CD90.2<sup>+</sup>ST2<sup>+</sup>KLRG1<sup>+</sup>, and lin<sup>-</sup>CD90.2<sup>+</sup>ST2<sup>-</sup>KLRG1<sup>+</sup>) were isolated from the lungs by sorting on a FACSARIA (Becton Dickinson) at the Flow Cytometry Facility of the University of Lausanne. Lin<sup>-</sup>CD90.2<sup>+</sup>ST2<sup>+</sup>KLRG1<sup>+</sup> ILC2s were either used immediately or collected in RNA later buffer (Invitrogen) or Trizol (Invitrogen).

### Lentiviral transduction and c-Maf quantification

Constructs with gRNA targeting c-Maf or luciferase were kindly provided by S. Notarbartolo and F. Sallusto (IRB, Bellinzona). The pALPS-GFP-miR30 vector was used for shRNA-mediated knock-down. Lentiviral particles were produced after transient co-transfection of HEK293FT cells with the shRNA- or gene-transfer vector, together with the packaging vectors psPAX2 (Addgene plasmid 12260) and pMD2.G (Addgene plasmid 12259), as described in (Aschenbrenner *et al*, 2018). Concentrated lentivirus was added to PHA-stimulated (PeproTech) *in vitro* expanded pure hILC2s (10<sup>5</sup> ILC2s/condition). After 24 h, and then every 2–3 days, half of the medium was removed and new fresh medium containing 200 U/ml rh-IL-2 and 20 ng/ml IL-7 (both from PeproTech) was added. After 10 days, GFP<sup>+</sup> ILC2s were sorted and tested for c-Maf expression by qPCR, as previously described (Ercolano *et al*, 2020a). Briefly, total RNA was extracted with TRIzol reagent (Invitrogen) and reverse transcribed using the iScript Reverse Transcription Supermix (Bio-Rad). The qPCR was carried out in the Applied Biosystems 7900HT Fast Real-Time PCR Sequence Detection System (Applied Biosystems) with MAF primers (5'-CTGGCAATGAGCAACTCCGA-3', 5'-AGCCGGTCATCCAGTAGTAGT-3') using KAPA SYBR FAST qPCR Kits (KK4601, Roche). The housekeeping gene (beta-2-microglobulin ( $\beta$ 2 M)) was used as an internal control to normalize the Ct values, using the 2<sup>- $\Delta$ Ct</sup> formula.

Then, hILC2s were further *in vitro* expanded for 2 weeks and tested for c-Maf expression by flow cytometry. c-Maf-deleted ILC2s (Maf-sh) and control (Luc-sh) were tested.

### Cytokine quantification

To evaluate secreted cytokines, human or mouse ILC2s (5,000 cells/ml) were incubated for 48 h in the presence of 20 U/ml IL-2 with or without 50 ng/ml IL-33 (Adipogen). After 48 h, cells were centrifuged and the supernatants were collected and immediately frozen. Cytokine concentration was evaluated by using the LEGENDplex™ kits (Biolegend) “human T Helper cytokine panel version 2” and “mouse T Helper cytokine panel version 3.” When comparing adult and cord blood ILC2s, cells were incubated for 3 h with PMA (250 ng/ml, Sigma) and Ionomycin (1  $\mu$ g/ $\mu$ l, Sigma) either immediately after cell sorting, or after an o.n. incubation in the presence of 50 ng/ml IL-33 (Adipogen). Samples were acquired on a Gallios flow cytometer (Beckman Coulter), and data were analyzed using the Legendplex software (version 8.0).

For intracellular cytokine staining, mILC2s were restimulated with PMA (30 ng/ml, Sigma) and Ionomycin (500 ng/ml, Sigma) for 3 h at 37°C in the presence of Golgi Stop (BD Biosciences). After staining for extracellular markers and viability using LIVE/DEAD™ Fixable Green Dead Cell Stain Kit (ThermoFisher Scientific), cells were fixed and permeabilized with the Foxp3 Transcription Factor Staining Buffer Set (eBiosciences) according to the manufacturer's instructions. Intracellular staining was performed in permeabilizing buffer using PE anti-mouse/human c-Maf (sym0F1, Invitrogen), PerCP-eF710 anti-human/mouse GATA3 (TWAJ, Invitrogen), PE-eF610 anti-mouse IL-13 (eBio13A, Invitrogen), BV711 anti-mouse IL-4 (11B11, Biolegend), and BV421 anti-mouse/human IL-5 (TRFK5, Biolegend). Data were acquired on a LSR II flow cytometer (BD) and analyzed with FlowJo software V10.

### Animal experiments

Id2-Cre<sup>ERT2</sup> mice were purchased from Jackson laboratories and crossed to Gata3<sup>fllox/fllox</sup> (Gata3<sup>fl/fl</sup>, Jackson Laboratory), to Maf<sup>fllox/fllox</sup> (Maf<sup>fl/fl</sup>) mice (Wende *et al*, 2012), or to Rosa-TdTomato reporter mice (B6. Cg-Gt(ROSA)26Sortm14(CAG-tdTomato)Hze/J; kindly provided by Prof. Werner Held) to generate Id2-Cre<sup>ERT2</sup> Gata3<sup>fl/fl</sup>, Id2-Cre<sup>ERT2</sup> Maf<sup>fl/fl</sup>, and Id2-Cre<sup>ERT2</sup>-TdTomato mice. To induce the Cre translocation, where indicated in the Figures, 1.5 mg/mouse/day of tamoxifen (Sigma) was injected i.p. for the indicated period. All animal experiments were performed in compliance with the University of Lausanne Institutional regulations and were approved by the veterinarian authorities of the Canton de Vaud (Authorizations VD3238, VD3455). The animals used were cohoused, and littermate were used in all experiments. All animals were included in the study.

### Histology and immunohistochemistry

Lungs were fixed with histological tissue fixative (Sigma), embedded in paraffin, and stained with hematoxylin and eosin by the Mouse Pathology Facility (University of Lausanne).

### RNA extraction, sequencing, and mRNAseq analysis

Whole RNA was extracted using the RNeasy Plus Micro Kit (Qiagen) according to the manufacturer's instructions. RNA quality was assessed using Fragment Analyzer System (Agilent) and RNA Kit

(Agilent). RNA samples were polyA-enriched, and libraries were prepared using the Illumina TruSeq<sup>®</sup> Stranded RNA kit. HiSeq 4000 single-end (150 bp) RNA sequencing runs (3 lanes) with a depth of approximately 20–30 million reads per sample were performed on an Illumina's Hi-Seq 2500 device at the Genomic Technologies Facility of the University of Lausanne.

Base calling, fastq file generation, and demultiplexing were performed using Illumina RTA v.1.18.66.3 and Illumina pipeline v.2.19.1. To remove adapter sequences and trim low-quality bases, raw sequencing reads were scanned using AdapterRemoval v.2.1.7 with parameters `-trimns` and `-trimqualities` (Schubert *et al*, 2016). Reads were aligned against the mouse GRCm38.95 reference genome using STAR v.2.6.0c (Dobin *et al*, 2013). Using samtools v.1.8 (Li *et al*, 2009), we converted sequence alignment map files to bam files and merged the aligned reads spread across 3 lanes of each sample into a single bam file per sample. Numbers of reads per gene were summarized using the `htseq-count` function of the HTSeq package v.0.9.1 (Anders *et al*, 2015). Computations were performed on the Vital-IT infrastructure of the Swiss Institute of Bioinformatics.

Subsequent statistical analyses were performed using R v.3.5.3. Raw counts were normalized using the trimmed mean of M values (TMM) method, and normalization factors were calculated using the `edgeR` package v.3.24.3 (Robinson *et al*, 2010). Counts were converted to  $\log_2$  counts per million (cpm) using the `voom` function implemented in the `limma` package v.3.38.3 (Ritchie *et al*, 2015). Differentially expressed genes between wild-type and knockout mILC2s were determined by fitting a linear model and computing moderated *t*-statistics using the `lmFit` and `eBayes` functions of the `limma` package. The *P*-value of each gene was adjusted using the Benjamini–Hochberg (BH) procedure. To determine whether significant genes were enriched in specific functions, we performed over-representation analysis of Gene Ontology biological process gene sets using the `enricher` function of the `clusterProfiler` package v.3.10.1 (Yu *et al*, 2012), separating up-regulated and down-regulated genes, and adjusting *P*-values using the BH procedure. We also used the `enricher` function to determine whether or not T helper signatures, CD8 T cell and Th2 memory signatures differed between *c-Maf*-depleted and wild-type mILC2s. Gene signatures consisted of Th1, Th2, and Th17 gene signatures (from Table EV1 of Lee *et al*, 2016), based on data by Stubbington *et al* (2015), genes up-regulated in memory versus naive CD8 T cells obtained from MSigDB (<https://www.gsea-msigdb.org/gsea/msigdb/index.jsp>) and genes over-expressed in murine lung ST2<sup>+</sup> Th2 cells (see Table EV2 for gene lists). Finally, a heatmap of gene z-scores across samples was generated using the `ComplexHeatmap` package v.1.1.20.0 (Gu *et al*, 2016).

### In silico search of the *c-Maf* binding motif

The sequences of the promoter regions of IL-4, IL-5, and IL-13 (including 100 base pairs upstream and downstream of promoters) were retrieved from the Eukaryotic Promoter Database (EPD (Dreos *et al*, 2017)). Regions of accessible chromatin upstream of these promoters were determined using ATAC-sequencing data obtained from ILC2s and Th2 cells sorted from mouse lungs (bigwig files downloaded from GEO, accession number: GSE77695; Shih *et al*, 2016). The *c-Maf* binding motif was retrieved from the MotifMap

database (Daily *et al*, 2011), and potential matches for this motif were identified using the FIMO tool of the MEME Suite v5.3.3 (Grant *et al*, 2011).

### ChIP assay

Expanded human and mouse ILC2s ( $n = 3$  adult healthy donors and  $n = 3$  mice injected 3 days with IL-33) were treated for 48 h with IL-2 or with IL-2 and IL-33. At the end of the stimulation, ILC2s were washed with PBS and cross-linked with 1% formaldehyde for 15 min. Chromatin was sheared by sonification with Bioruptor Pico (30" on and 30" off for 25 cycles) and immunoprecipitated with anti-*c-Maf* (5  $\mu$ g, Diagenode) or an isotype control IgG using MAG-nify Chromatin Immunoprecipitation system (Thermo Fisher). Eluted DNA was used for qPCR analysis using hIL-13 (5'-CCTCATGGCGCTTTTGTGAC-3', 5'-TCTGGTTCTGGGTGATGTTGA-3'), hIL-5 (5'-ATCATCGTGGCGCATGTATTAC-3', 5'-AAAGAACTTGAGCAAACCAGT-3') and hIL-4 (5'-CCAACTGCTCCCCCTCTG-3', 5'TCTGTTACGGTCAACTCGGTG-3') primers, and mIL-13 (5'-GAAGGCTCCGCTCTGCAAT-3', 5'-TCCAGGCTGCACAGTACA-3'), mIL-5 (5'-TCAGGGGCTAGACATACTGAAG-3', 5'-CCAAGGAAGCTTGCA GGTAAT-3') and mIL-4 (5'-CCCCAGCTAGTTGTCATCCTG-3', 5'-CAAGTGATTTTGTGCGCATCCG-3') primers, as previously shown (Ercolano *et al*, 2021).

### Statistics

GraphPad Prism software was used to perform statistical analyses. Shapiro–Wilk test was applied to determine normal distribution. Tests used are specified in the legend of each Figure. The data are shown by plotting individual data points, and the mean  $\pm$  SEM.  $P < 0.05$  was considered statistically significant and labeled with \* $P < 0.01$  labeled with \*\* $P < 0.001$  with \*\*\* and  $P < 0.0001$  with \*\*\*\*. Experiments were analyzed in a blinded way, without knowing the genotype of the animals or the status of the human primary cells used.

## Data availability

The RNA sequencing data have been deposited in NCBI's Gene Expression Omnibus (GEO) and are accessible through accession number GSE166739 (<https://www.ncbi.nlm.nih.gov/geo/query/acc.cgi?acc=GSE166739>).

**Expanded View** for this article is available online.

### Acknowledgments

This work was funded by the University of Lausanne and grants from the Max Cloëtta Foundation (G.V.), the Swiss National Foundation (G.V.: 310030\_182680; C.J.: PRIMA PR00P3\_179727), the Helmut Horten Foundation (C.J.), the Umberto Veronesi Foundation (G.E.), Bologna AIL (Associazione Italiana contro le Leucemie)/Section of Bologna, FATRO/Foundation Corrado and Bruno Maria Zaini-Bologna, Fabbri1905. Open access funding provided by Université de Lausanne.

### Author contributions

**Sara Trabanelli:** Conceptualization; Data curation; Formal analysis; Supervision; Investigation; Writing—original draft; Writing—review and editing.

**Giuseppe Ercolano:** Investigation. **Tania Wyss:** Software; Formal analysis; Investigation. **Alejandra Gomez-Cadena:** Investigation. **Maryline Falquet:** Investigation. **Daniela Cropp:** Investigation. **Claire Imbratta:** Investigation. **Marine M Leblond:** Investigation. **Valentina Salvestrini:** Resources. **Antonio Curti:** Resources. **Olivier Adotevi:** Resources. **Camilla Jandus:** Conceptualization; Data curation; Formal analysis; Supervision; Funding acquisition; Writing—original draft; Project administration; Writing—review and editing. **Grégory Verdeil:** Conceptualization; Resources; Data curation; Formal analysis; Supervision; Funding acquisition; Investigation; Methodology; Writing—original draft; Project administration; Writing—review and editing.

In addition to the CRediT author contributions listed above, the contributions in detail are:

ST, CJ, and GV conceived, designed the experiments, and analyzed the results. ST, GV, GE, AG-C, DC, MML, MF, and CI performed the experiments. TW performed the RNA-seq data analysis. VS, AC, and OA provided the cord blood samples. ST, CJ, and GV wrote the manuscript. All the authors critically discussed the results and reviewed the manuscript.

### Disclosure and competing interests statement

The authors declare that they have no conflict of interest.

## References

- Anders S, Pyl PT, Huber W (2015) HTSeq—a Python framework to work with high-throughput sequencing data. *Bioinformatics* 31: 166–169
- Aschenbrenner D, Foglierini M, Jarrossay D, Hu D, Weiner HL, Kuchroo VK, Lanzavecchia A, Notarbartolo S, Sallusto F (2018) An immunoregulatory and tissue-residency program modulated by c-MAF in human TH17 cells. *Nat Immunol* 19: 1126–1136
- Bekkering S, Arts RJW, Novakovic B, Kourtzelis I, van der Heijden CDCC, Li Y, Popa CD, ter Horst R, van Tuijl J, Netea-Maier RT et al (2018) Metabolic induction of trained immunity through the mevalonate pathway. *Cell* 172: 135–146
- Bernink JH, Ohne Y, Teunissen MBM, Wang J, Wu J, Krabbendam L, Guntermann C, Volckmann R, Koster J, van Tol S et al (2019) c-Kit-positive ILC2s exhibit an ILC3-like signature that may contribute to IL-17-mediated pathologies. *Nat Immunol* 20: 992–1003
- Bjorklund AK, Forkel M, Picelli S, Konya V, Theorell J, Friberg D, Sandberg R, Mjosberg J (2016) The heterogeneity of human CD127(+) innate lymphoid cells revealed by single-cell RNA sequencing. *Nat Immunol* 17: 451–460
- Colonna M (2018) Innate lymphoid cells: diversity, plasticity, and unique functions in immunity. *Immunity* 48: 1104–1117
- Daily K, Patel VR, Rigor P, Xie X, Baldi P (2011) MotifMap: integrative genome-wide maps of regulatory motif sites for model species. *BMC Bioinformatics* 12: 495
- Dobin A, Davis CA, Schlesinger F, Drenkow J, Zaleski C, Jha S, Batut P, Chaisson M, Gingeras TR (2013) STAR: ultrafast universal RNA-seq aligner. *Bioinformatics* 29: 15–21
- Dominguez-Andres J, Netea MG (2020) The specifics of innate immune memory. *Science* 368: 1052–1053
- Dreos R, Ambrosini G, Groux R, Cavin Perier R, Bucher P (2017) The eukaryotic promoter database in its 30th year: focus on non-vertebrate organisms. *Nucleic Acids Res* 45: D51–D55
- Ercolano G, Garcia-Garijo A, Salomé B, Gomez-Cadena A, Vanoni G, Mastelic-Gavillet B, Ianaro A, Speiser DE, Romero P, Trabanelli S et al (2020a) Immunosuppressive mediators impair proinflammatory innate lymphoid cell function in human malignant melanoma. *Cancer Immunol Res* 8: 556–564
- Ercolano G, Gomez-Cadena A, Dumauthioz N, Vanoni G, Kreutzfeldt M, Wyss T, Michalik L, Loyon R, Ianaro A, Ho PC et al (2021) PPAR drives IL-33-dependent ILC2 pro-tumoral functions. *Nat Commun* 12: 2538
- Ercolano G, Wyss T, Salome B, Romero P, Trabanelli S, Jandus C (2020b) Distinct and shared gene expression for human innate versus adaptive helper lymphoid cells. *J Leukoc Biol* 108: 723–737
- Ferreira ACF, Szeto ACH, Heycock MWD, Clark PA, Walker JA, Crisp A, Barlow JL, Kitching S, Lim A, Gogoi M et al (2021) RORalpha is a critical checkpoint for T cell and ILC2 commitment in the embryonic thymus. *Nat Immunol* 22: 166–178
- Gabryšová L, Alvarez-Martinez M, Luisier R, Cox LS, Sodenkamp J, Hosking C, Pérez-Mazliah D, Whicher C, Kannan Y, Potempa K et al (2018) c-Maf controls immune responses by regulating disease-specific gene networks and repressing IL-2 in CD4(+) T cells. *Nat Immunol* 19: 497–507
- Giordano M, Henin C, Maurizio J, Imbratta C, Bourdely P, Buferne M, Baitsch L, Vanhille L, Sieweke MH, Speiser DE et al (2015) Molecular profiling of CD8 T cells in autochthonous melanoma identifies Maf as driver of exhaustion. *EMBO J* 34: 2042–2058
- Grant CE, Bailey TL, Noble WS (2011) FIMO: scanning for occurrences of a given motif. *Bioinformatics* 27: 1017–1018
- Gu Z, Eils R, Schlesner M (2016) Complex heatmaps reveal patterns and correlations in multidimensional genomic data. *Bioinformatics* 32: 2847–2849
- Halim TY, MacLaren A, Romanish MT, Gold MJ, McNagny KM, Takei F (2012) Retinoic-acid-receptor-related orphan nuclear receptor alpha is required for natural helper cell development and allergic inflammation. *Immunity* 37: 463–474
- Harly C, Cam M, Kaye J, Bhandoola A (2018) Development and differentiation of early innate lymphoid progenitors. *J Exp Med* 215: 249–262
- Ho IC, Hodge MR, Rooney JW, Glimcher LH (1996) The proto-oncogene c-maf is responsible for tissue-specific expression of interleukin-4. *Cell* 85: 973–983
- Hochdorfer T, Winkler C, Pardali K, Mjosberg J (2019) Expression of c-Kit discriminates between two functionally distinct subsets of human type 2 innate lymphoid cells. *Eur J Immunol* 49: 884–893
- Howard E, Lewis G, Galle-Treger L, Hurrell BP, Helou DG, Shafiei-Jahani P, Painter JD, Muench GA, Soroosh P, Akbari O (2020) IL-10 production by ILC2s requires Blimp-1 and cMaf, modulates cellular metabolism, and ameliorates airway hyperreactivity. *J Allergy Clin Immunol* 147: 1281–1295
- Howard E, Lewis G, Galle-Treger L, Hurrell BP, Helou DG, Shafiei-Jahani P, Painter JD, Muench GA, Soroosh P, Akbari O (2021) IL-10 production by ILC2s requires Blimp-1 and cMaf, modulates cellular metabolism, and ameliorates airway hyperreactivity. *J Allergy Clin Immunol* 147: 1281–1295
- Hoyler T, Klose CS, Souabni A, Turqueti-Neves A, Pfeifer D, Rawlins EL, Voehringer D, Busslinger M, Diefenbach A (2012) The transcription factor GATA-3 controls cell fate and maintenance of type 2 innate lymphoid cells. *Immunity* 37: 634–648
- Huang Y, Guo L, Qiu J, Chen X, Hu-Li J, Siebenlist U, Williamson PR, Urban Jr JF, Paul WE (2015) IL-25-responsive, lineage-negative KLRG1(hi) cells are multipotential 'inflammatory' type 2 innate lymphoid cells. *Nat Immunol* 16: 161–169
- Imbratta C, Leblond MM, Bouzourene H, Speiser DE, Velin D, Verdeil G (2019) Maf deficiency in T cells dysregulates Treg - TH17 balance leading to spontaneous colitis. *Sci Rep* 9: 6135
- Ishizuka IE, Constantinides MG, Gudjonson H, Bendelac A (2016) The innate lymphoid cell precursor. *Annu Rev Immunol* 34: 299–316

- Kim JI, Ho IC, Grusby MJ, Glimcher LH (1999) The transcription factor c-Maf controls the production of interleukin-4 but not other Th2 cytokines. *Immunity* 10: 745–751
- Lee YJ, Starrett GJ, Lee ST, Yang R, Henzler CM, Jameson SC, Hogquist KA (2016) Lineage-specific effector signatures of invariant NKT cells are shared amongst gammadelta T, innate lymphoid, and Th cells. *J Immunol* 197: 1460–1470
- Li H, Handsaker B, Wysoker A, Fennell T, Ruan J, Homer N, Marth G, Abecasis G, Durbin R (2009) The sequence alignment/map format and SAMtools. *Bioinformatics* 25: 2078–2079
- Lim AI, Li Y, Lopez-Lastra S, Stadhouders R, Paul F, Casrouge A, Serafini N, Puel A, Bustamante J, Surace L et al (2017) Systemic human ILC precursors provide a substrate for tissue ILC differentiation. *Cell* 168: 1086–1100
- Martinez-Gonzalez I, Matha L, Steer CA, Ghaedi M, Poon GF, Takei F (2016) Allergen-experienced group 2 innate lymphoid cells acquire memory-like properties and enhance allergic lung inflammation. *Immunity* 45: 198–208
- Neumann C, Blume J, Roy U, Teh PP, Vasanthakumar A, Beller A, Liao Y, Heinrich F, Arenzana TL, Hackney JA et al (2019) c-Maf-dependent Treg cell control of intestinal TH17 cells and IgA establishes host-microbiota homeostasis. *Nat Immunol* 20: 471–481
- Parker ME, Barrera A, Wheaton JD, Zuberbuehler MK, Allan DSJ, Carlyle JR, Reddy TE, Ciofani M (2020) c-Maf regulates the plasticity of group 3 innate lymphoid cells by restraining the type 1 program. *J Exp Med* 217: e20191030
- Pokrovskii M, Hall JA, Ochayon DE, Yi R, Chaimowitz NS, Seelamneni H, Carriero N, Watters A, Waggoner SN, Littman DR et al (2019) Characterization of transcriptional regulatory networks that promote and restrict identities and functions of intestinal innate lymphoid cells. *Immunity* 51: 185–197
- Rahimi RA, Nepal K, Cetinbas M, Sadreyev RI, Luster AD (2020) Distinct functions of tissue-resident and circulating memory Th2 cells in allergic airway disease. *J Exp Med* 217: e20190865
- Ritchie ME, Phipson B, Wu D, Hu Y, Law CW, Shi W, Smyth GK (2015) limma powers differential expression analyses for RNA-sequencing and microarray studies. *Nucleic Acids Res* 43: e47
- Robinson JT, Thorvaldsdottir H, Winckler W, Guttman M, Lander ES, Getz G, Mesirov JP (2011) Integrative genomics viewer. *Nat Biotechnol* 29: 24–26
- Robinson MD, McCarthy DJ, Smyth GK (2010) edgeR: a Bioconductor package for differential expression analysis of digital gene expression data. *Bioinformatics* 26: 139–140
- Schubert M, Lindgreen S, Orlando L (2016) AdapterRemoval v2: rapid adapter trimming, identification, and read merging. *BMC Res Notes* 9: 88
- Shih HY, Sciume G, Mikami Y, Guo L, Sun HW, Brooks SR, Urban Jr JF, Davis FP, Kanno Y, O'Shea JJ (2016) Developmental acquisition of regulomes underlies innate lymphoid cell functionality. *Cell* 165: 1120–1133
- Stubbington MJ, Mahata B, Svensson V, Deonaraine A, Nissen JK, Betz AG, Teichmann SA (2015) An atlas of mouse CD4(+) T cell transcriptomes. *Biol Direct* 10: 14
- Tizian C, Lahmann A, Holsken O, Cosovanu C, Kofoed-Branzk M, Heinrich F, Mashreghi MF, Kruglov A, Diefenbach A, Neumann C (2020) c-Maf restrains T-bet-driven programming of CCR6-negative group 3 innate lymphoid cells. *Elife* 9: e52549
- Vivier E, Artis D, Colonna M, Diefenbach A, Di Santo JP, Eberl G, Koyasu S, Locksley RM, McKenzie ANJ, Mebius RE et al (2018) Innate lymphoid cells: 10 years on. *Cell* 174: 1054–1066
- Wende H, Lechner SG, Cheret C, Bourane S, Kolanczyk ME, Pattyn A, Reuter K, Munier FL, Carroll P, Lewin GR et al (2012) The transcription factor c-Maf controls touch receptor development and function. *Science* 335: 1373–1376
- Xu M, Pokrovskii M, Ding Y, Yi R, Au C, Harrison OJ, Galan C, Belkaid Y, Bonneau R, Littman DR (2018) c-MAF-dependent regulatory T cells mediate immunological tolerance to a gut pathobiont. *Nature* 554: 373–377
- Yu G, Wang LG, Han Y, He QY (2012) clusterProfiler: an R package for comparing biological themes among gene clusters. *OMICS* 16: 284–287
- Yu Y, Wang C, Clare S, Wang J, Lee S-C, Brandt C, Burke S, Lu L, He D, Jenkins NA et al (2015) The transcription factor Bcl11b is specifically expressed in group 2 innate lymphoid cells and is essential for their development. *J Exp Med* 212: 865–874
- Zhang K, Xu X, Pasha MA, Siebel CW, Costello A, Haczku A, MacNamara K, Liang T, Zhu J, Bhandoola A et al (2017) Cutting edge: notch signaling promotes the plasticity of group-2 innate lymphoid cells. *J Immunol* 198: 1798–1803
- Zhu Y, Liu Y, Zhu X, Wang Z, Wang M (2020) Upregulation of miR-155 regulates group 2 innate lymphoid cells by targeting c-maf in allergic rhinitis. *Eur J Pharmacol* 887: 173564



**License:** This is an open access article under the terms of the Creative Commons Attribution-NonCommercial-NoDerivs License, which permits use and distribution in any medium, provided the original work is properly cited, the use is non-commercial and no modifications or adaptations are made.